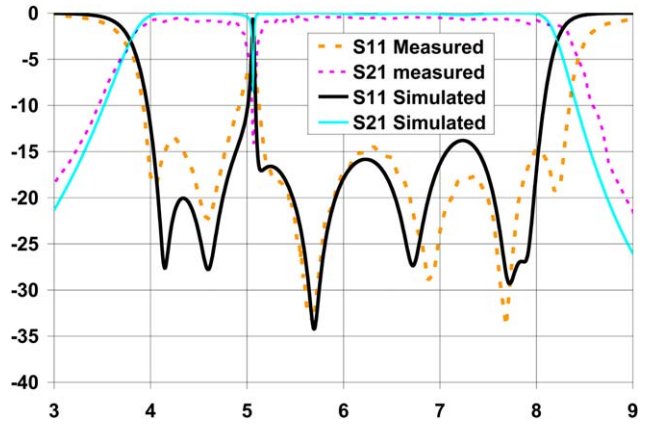

Figure 8 Measured performance of the filter with one transmission zero in the passband. [Color figure can be viewed in the online issue, which is available at wileyonlinelibrary.com]

It is also possible to add more than one resonators in the filter. Figure 6 shows another filter with two resonators added to the original filter. The resonant frequency and coupling strength of these two resonators can be adjusted independently to achieve two transmission zeros at different frequencies with different stopband widths. An example of the simulated result is shown in Figure 7. It can be seen that two transmission zeros are realized at 4.81 and 6.74, GHz respectively, while the frequency response of the filter at other frequencies is not significantly changed.

4. EXPERIMENTAL RESULTS

To validate the above theory, the filter shown in Figure 3 was fabricated and tested. The measured performance is shown in Figure 8, compared with the simulated result. The transmission zero is easily observed in the passband of the filter at 5.06 GHz. An attenuation of 14 dB is achieved in this region. The measured performance agrees well with the simulation. By comparing the measured results of the filter shown in Figure 8 and the original results shown in Figure 2, it can be seen that, apart from the transmission zero introduced, the filter performance is hardly changed at other frequencies.

5. CONCLUSIONS AND FUTURE WORK

In this article, the design of a wideband filter is briefed. By adding one or more extra resonators weakly coupled to the filter, one transmission zero can be introduced by each extra resonator and a relatively narrow stopband can be realized. These extra resonators have little effect on the filter at other frequencies.

As mentioned in the article, the extra resonators will affect the performance of the filter if the coupling is comparable to the internal couplings of the original filter. In the future work, it would be interesting to establish the synthesis/optimization algorithm, taking the extra resonator and its coupling strength to the filter into account when designing the filter, so that wider stopband can be achieved while maintaining good performance at other frequencies. As the extra resonator is independent from the filter, it is also possible to combine this idea with MEMS technology or other method to realize tunable stopband in the passband of broadband filters.

ACKNOWLEDGMENT

The authors would like to thanks Professor Michael Lancaster at the University of Birmingham, UK and Dr. Guoyong Zhang for useful discussion. Some of the initial work was carried out when one author was with the University of Birmingham.

REFERENCES

1. K.W. Wong, L. Chiu, and Q. Xue, Wideband parallel-strip bandpass filter using phase inverter, IEEE Microwave Wireless Components Lett 18 (2008), 503–505.
2. S. Sun, L. Zhu, and H.-H. Tan, A compact wideband bandpass filter using transversal resonator and asymmetrical interdigital coupled lines, IEEE Microwave Wireless Components Lett 18 (2008), 173–175.
3. L. Zhu, H. Bu, and K. Wu, Broadband and compact multi-pole microstrip bandpass filters using ground plane aperture technique, IEEE Proc Microwave Antennas Propag 149 (2002), 71–77.
4. H. Shaman, and J.-S. Hong, Input and output cross-coupled wideband bandpass filter, IEEE Trans Microwave Theory Tech 55 (2007), 2562–2568.
5. A. Martin, M. El Sabbagh, and B. Mohajer-Iravani, A miniaturized ultra-wideband microstrip filter using interdigital capacitive loading and interresonator tapped-in coupling, In: IEEE Int Conf Ultra-Wideband (ICUWB), 2012, pp. 95–98.
6. G. Zhang, M.J. Lancaster, F. Huang, and N. Roddis, A superconducting microstrip bandstop filter for an L-band radio telescope receiver, In: European Microwave Conference, Volume 1, October 4–6, Paris, France, 2005, p. 4.
7. G. Zhang, M.J. Lancaster, F. Huang, Y. Pan, and N. Roddis, Wideband microtrip bandpass filters for radio astronomy applications, 36th European Microwave Conference, Manchester, UK, September 2006, pp. 661–663.
8. A.M. Abu-Hudrouss, A.B. Jayyousi, and M.J. Lancaster, Triple-band HTS filter using dual spiral resonators with capacitive-loading, IEEE Trans on Appl Superconductivity, 18 (2008), 1728–1732.
9. G. Matthaei, L. Young, and E.M.T. Jones, Micorwave Filters, Impedance-Matching Networks and Coupling Structure, Artech, Norwood, MA, 1980.
10. Sonnet Software, EM User's Manual, Version 9.52; Sonnet Software, Inc., Liverpool, NY, 2005.
11. F. Huang, Ultra-compact superconducting narrow-band filter using single- and twin-spiral resonators, In: IEEE Trans. Microwave Theory Tech, February 2003, pp. 487–491.

DISCRETE GREEN'S FUNCTION APPROACH FOR THE ANALYSIS OF A DUAL BAND-NOTCHED UWB ANTENNA

Salma Mirhadi, Mohammad Soleimani, and Ali Abdolali
Department of Electrical Engineering, Iran University of Science and Technology, P. O. Box 1684613114, Narmak, Tehran, Iran; Corresponding author: s_mirhadi@iust.ac.ir

Received 3 February 2013

ABSTRACT: *A novel UWB monopole antenna with trident feeding and dual band-notched characteristics is proposed. The antenna consists of two bottom corner notches for improvement of impedance matching and two U-shaped slots for rejection of WLAN and WiMAX bands. Discrete Green's function approach has been utilized to numerically achieve time-domain current distribution on the antenna. A good agreement between simulation and experimental results is observed.* © 2013 Wiley Periodicals, Inc.
Microwave Opt Technol Lett 55:2168–2174, 2013; View this article online at wileyonlinelibrary.com. DOI 10.1002/mop.27784

Key words: *DGF; dual band-notched; trident feeding; U-shaped slots; UWB antennas*

1. INTRODUCTION

Bandwidth enhancement of square planar metal plate monopole antenna has been considerably investigated due to the simplicity

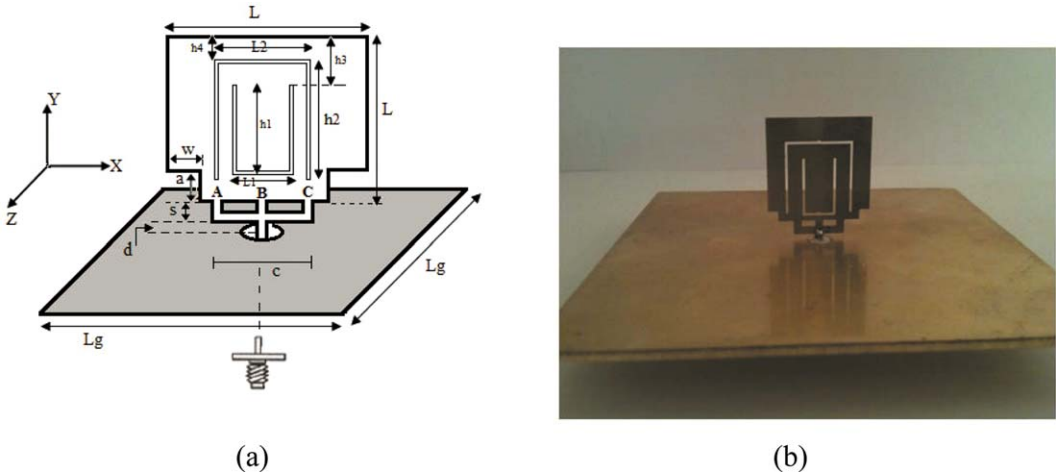

Figure 1 The proposed antenna (a) geometry and (b) photograph. [Color figure can be viewed in the online issue, which is available at wileyonlinelibrary.com]

of the construction of this type of antenna and maintenance of the radiation pattern within the whole impedance bandwidth [1–4]. One of the techniques for bandwidth enhancement is the use of triple feeding which is based on the achievement of a much more uniform current distribution than that of the single feeding antenna [5]. However, designing slots on the antenna with multiple feeding for band notched characteristics is more difficult than that with single feeding due to the fact that control of the current distribution in the multiple feeding antenna is more effortful than that in the single feeding antenna. In this article, we have designed two U-shaped slots for the trident feeding UWB antenna in a manner that affect three feeding locations. Furthermore, we have selected discrete Green's function (DGF) method as a simulation tool for the analysis of the antenna. The dyadic finite-difference time domain (FDTD) compatible Green's function, referred to as the DGF, has been proposed by Vazquez and Parini in 1999 [6]. Despite the fact that antenna modeling using DGF method has been presented in [7] and [8], this technique has received little attention in the analysis of the various antenna, especially, antenna with more than one dimension. In fact, DGF method is a combination of the method of moments and FDTD. On the one hand, DGF method has the advantage of the moments method that the computations are only performed on the antenna regardless of the free space nodes around it. On the other hand, this technique has the advantage of the FDTD method that computes time domain characteristics of the antenna, and the broadband frequency behavior of the antenna has been attained with a single run of the written code. It is the first time that the DGF method is used for the analysis of the UWB antenna.

2. ANTENNA DESIGN

The proposed antenna and a photograph of the fabricated prototype are shown in Figure 1. It is a square planar monopole antenna of side L having trident feeding and two bottom corner notches with dimension $a \times w$. Cutting notches at the bottom edges of the antenna lead to alleviate of horizontal current (J_x), which rarely contribute to the radiation. The width of all feeding strips is assumed 1.5 mm. The antenna has been fabricated using 0.2 mm brass sheet mounted above a ground plane of size 80×80 mm^2. The antenna is fed by a 50-Ω coaxial probe behind the ground plane.

Two U-shaped slots have been implemented on the antenna to realize band notched characteristic. The U-shaped slot has been designed for WLAN band (5.15–5.85 GHz) rejection, and the inverted U-shaped slot is also considered for the WiMAX band rejection (3.3–3.7 GHz). The dimensions of the slot are selected so that the center of the rejected frequency band satisfies $f_{\text{notch\_1,2}} = c/(4h_{1,2}+2L_{1,2}-4t)$, where c is the speed of light and t is the width of the slot assumed 0.5 mm. Figure 2 shows the surface current distribution over the antenna at 3.5 and 5.5 GHz. The current is concentrated around the edge of the slot represented as a short-circuit stub. As the half length of the slot is approximately $\lambda/4$, at 5.5 GHz, short circuit at the end of U-shaped slot becomes open circuit at the central feeding point (point B), which leads to impedance mismatching. The short circuit at the end of the inverted U-slot causes the antenna has seen nearly zero impedance at the feeding point A and C and which, in turn, leads to impedance mismatching. The optimum designed parameters are listed in Table 1.

3. FORMULATION OF DGF METHOD

Scattered electric field of an antenna in the spatial steps $(i,j,k) = (i\Delta x, j\Delta y, k\Delta z)$ and at the time step $(n\Delta t)$ can be obtained using the convolution of the current induced on the antenna and DGFs as:

$$\left[\vec{E}_{\text{scat}}\right]^n_{i,j,k} = \sum_{n'=0}^{n} \sum_{i',j',k'} [\bar{\text{G}}]^{n-n'}_{i-i',j-j',k-k'} \left[\vec{J}\right]^{n'}_{i',j',k'}$$
$$i,j,k \text{ any where but } i',j',k' \text{ on the antenna} \quad (1)$$

where $[\bar{\text{G}}]$ is the dyadic DGF and can be obtained through the relationship with the scalar DGF [7]. As explained in [7], the scalar DGF is the solution of the second order central difference approximation of the scalar wave equation with Kronecker delta excitation expressed as (it has been considered as $i' = j' = k' = n' = 0$ due to the shifting capability of the Green's functions):

$$\frac{g^{n+1}_{i,j,k} - 2g^{n}_{i,j,k} + g^{n-1}_{i,j,k}}{c^2(\Delta t)^2} - \frac{g^{n}_{i+1,j,k} - 2g^{n}_{i,j,k} + g^{n}_{i-1,j,k}}{(\Delta x)^2} - \frac{g^{n}_{i,j+1,k} - 2g^{n}_{i,j,k} + g^{n}_{i,j-1,k}}{(\Delta y)^2} - \frac{g^{n}_{i,j,k+1} - 2g^{n}_{i,j,k} + g^{n}_{i,j,k-1}}{(\Delta z)^2} = \delta^{n-n'}_{i-i',j-j',k-k'} \quad (2)$$

The solution of Eq. (2) can be achieved using multidimensional z-transform as [7]:

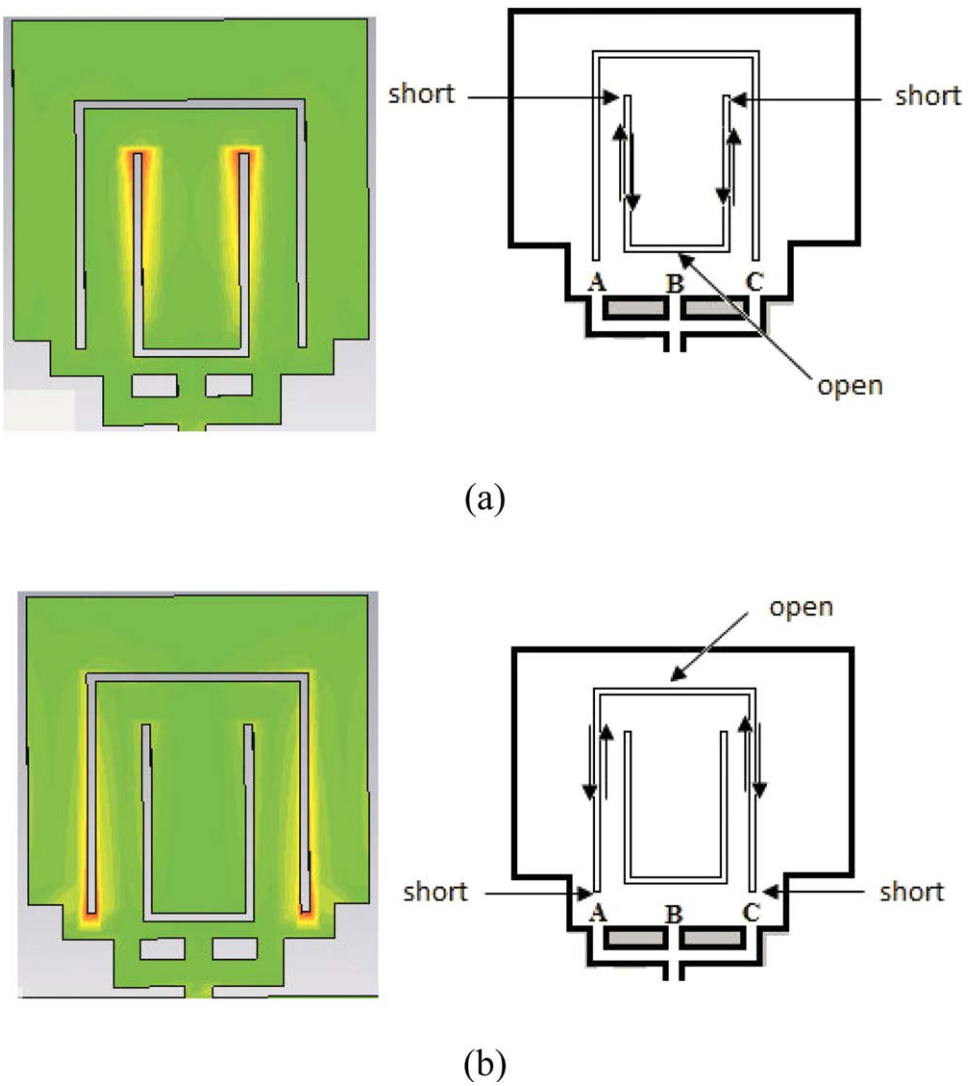

Figure 2 The current amplitude distribution (a) at 5.5 GHz and (b) at 3.5 GHz. [Color figure can be viewed in the online issue, which is available at wileyonlinelibrary.com]

$$g_{i,j,k}^{n+1} = \sum_{m=0}^{n/2} (-1)^m \binom{n-m}{m} \cdot \sum \left(n-2m; p_x, p_y, p_z\right) \prod_{\substack{t=i,j,k \\ s=x,y,z}} \alpha_s^{p_s} J_{p_s-l}^{(l,l)}(\xi_s)(R_{2s}-R_{1s})^{p_s-l} \tag{3}$$

where

$$\alpha_s = \frac{c^2\Delta t^2}{\Delta s^2},\ \beta_s = \frac{3\alpha_s - 1}{3\alpha_s},\ R_{1,2s} = \beta_s \pm \sqrt{\beta_s{}^2 - 1}$$

$$\xi_s = \frac{R_{1s}+R_{2s}}{R_{1s}-R_{2s}},\ \left(n-2m; p_x, p_y, p_z\right) = \frac{(n-2m)!}{p_x!p_y!p_z!}$$

and $J_n^{(\alpha,\beta)}(\xi)$ is the orthogonal Jacobi polynomial. Owing to the fact that the sum of the incident and scattered electric fields on the electric conductor antenna must vanish, we can write:

$$\left[\vec{E}_{\text{scat}}\right]_{i,j,k}^{n} + \left[\vec{E}_{\text{inc}}\right]_{i,j,k}^{n} = 0 \qquad i,j,k \text{ on the antenna}$$

TABLE 1 The Optimum Designed Parameters of the Proposed Antenna

Parameter	L	a	w	d	c	s	L	h_2	h_1	L_2	L_1	h_3	h_4
Optimum Value (mm)	20	2	2	1	10	2.8	20	14	11.5	13	6.5	7.5	4.5

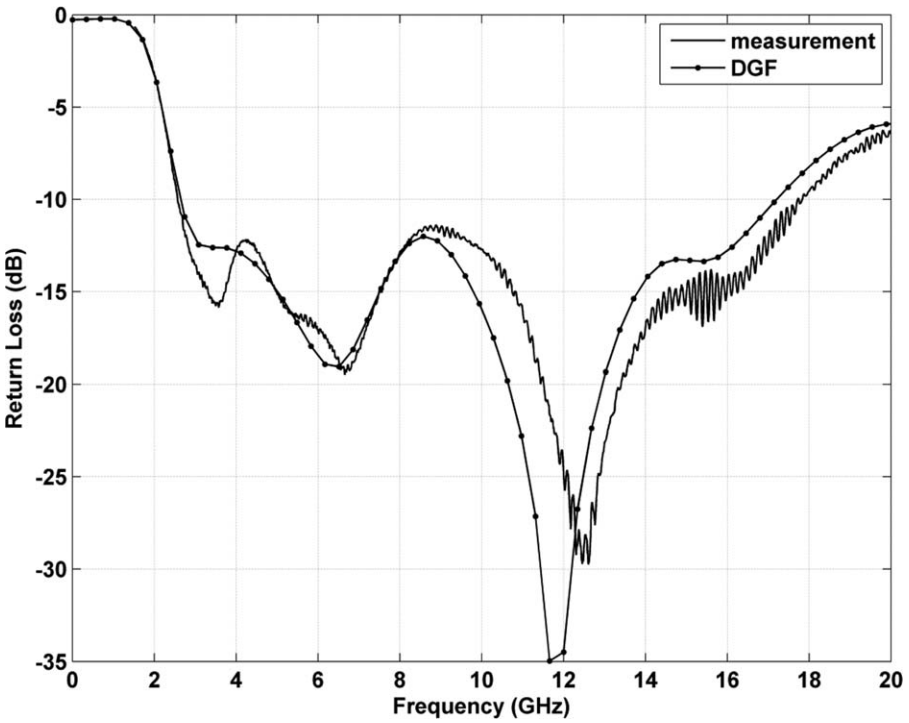

Figure 3 Simulated and measured return loss of the antenna of Figure 1 without slots

$$\sum_{n'=0}^{n}\sum_{i',j',k'}[\bar{\mathrm{G}}]^{n-n'}_{i-i',j-j',k-k'}\left[\vec{J}\right]^{n'}_{i',j',k'}+\left[\vec{E}_{\mathrm{inc}}\right]^{n}_{i,j,k}=0$$

$$i,j,k,i',j',k' \text{ on the antenna} \qquad (4)$$

As the induced current on the antenna is unknown, Eq. (4) must be inverted in order to obtain the update equation for the electric current on the antenna. It can be achieved using the property of the zero time step DGF which occurs at $n=n'$ and is equal to spatial delta Kroneker function. Therefore, the time step $n=n'$ can be considered separately from the rest of the time steps resulting in the following:

$$\left[\vec{J}\right]^{n}_{i,j,k}=\varepsilon\left[\vec{E}_{\mathrm{inc}}\right]^{n}_{i,j,k}+\varepsilon\sum_{n'=0}^{n-1}\sum_{i',j',k'}[\bar{G}]^{n-n'}_{i-i',j-j',k-k'}\left[\vec{J}\right]^{n'}_{i',j',k'}$$

$$i,j,k,i',j',k' \text{ on the antenna} \qquad (5)$$

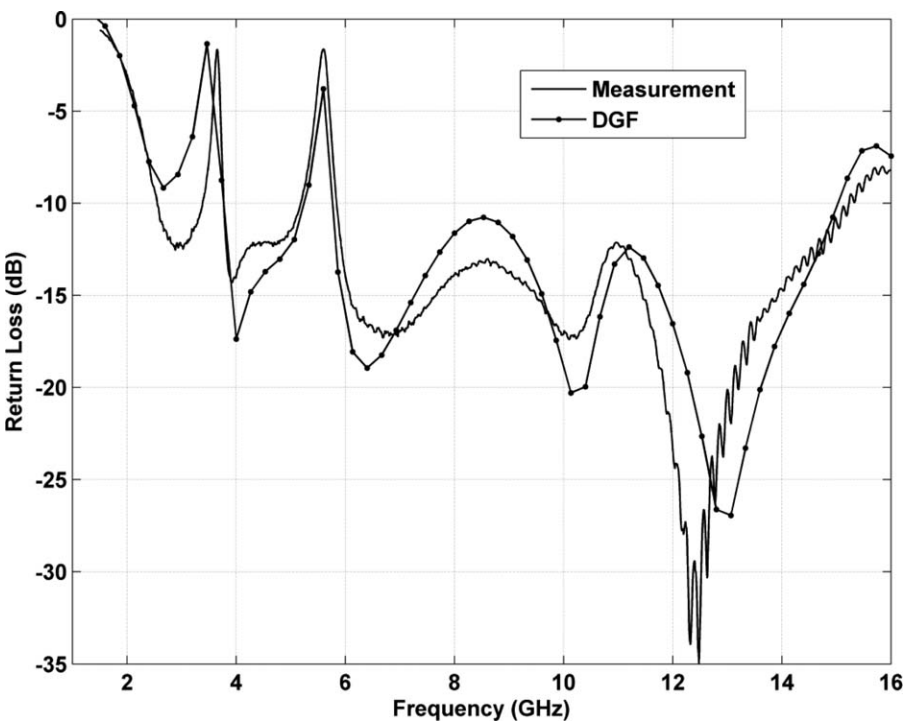

Figure 4 Simulated and measured return loss of antenna of Figure 1

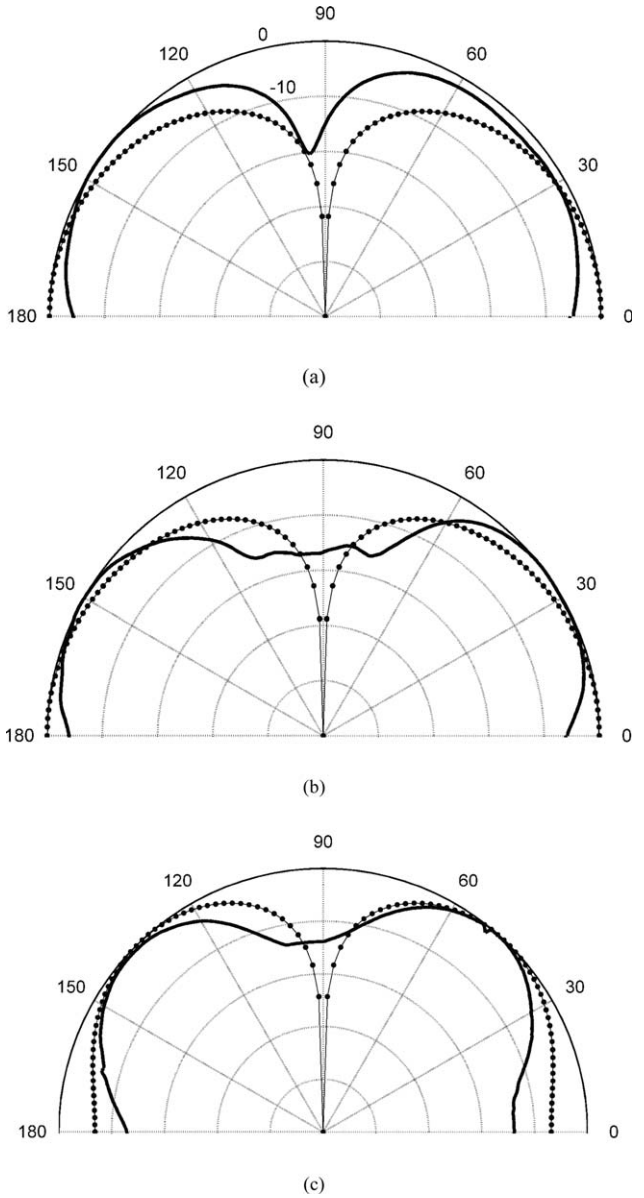

Figure 5 Simulated and measured pattern of the antenna in *x-y* plane at (a) 3 GHz, (b) 6.5 GHz, and (c) 9 GHz. (solid line: measurement, dotted line: simulation)

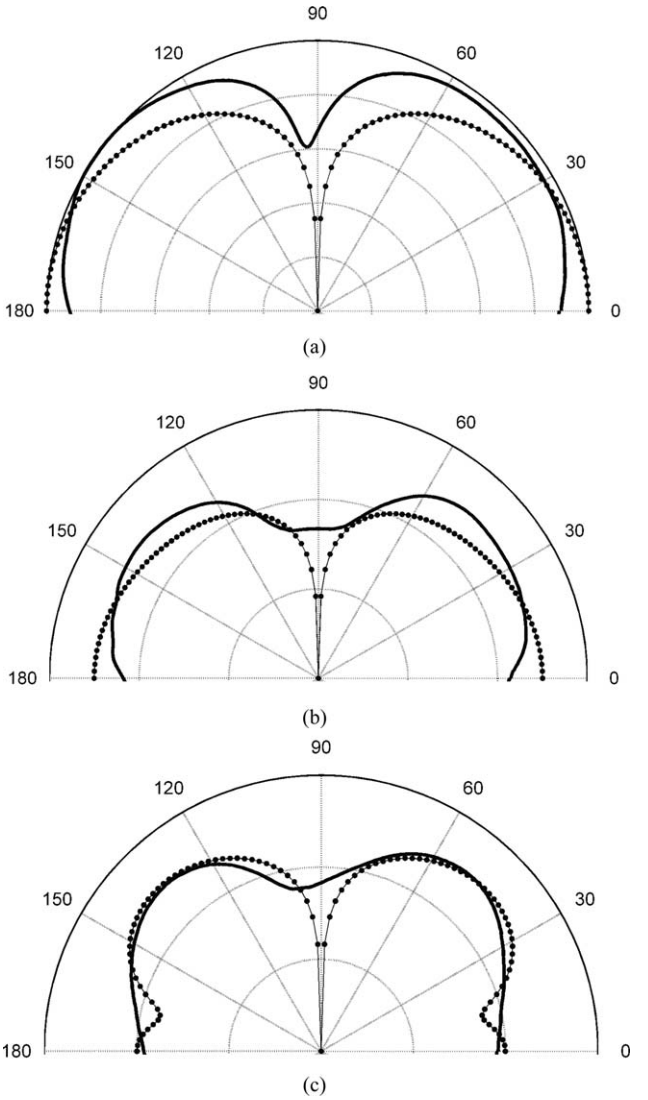

Figure 6 Simulated and measured pattern of the antenna in *y-z* plane at (a) 3 GHz, (b) 6.5 GHz, and (c) 9 GHz. (solid line: measurement, dotted line: simulation)

In the modeling of the proposed antenna using DGF, we have considered an infinite ground plane and the currents are calculated only on the antenna. For this purpose, the DGFs of the semi-infinite space, in the *x-y* plane, for the coordinates as shown in Figure 1, must be achieved as Eq. (6) by the application of the image theory regardless of the antenna thickness.

$$
\begin{aligned}
G_{IM_{xx}}^{n-n'}(i-i',j,j') &= G_{xx}^{n-n'}(i-i',j-j',0) - G_{xx}^{n-n'}(i-i',j+j',0)\\
G_{IM_{yy}}^{n-n'}(i-i',j,j') &= G_{yy}^{n-n'}(i-i',j-j',0) + G_{yy}^{n-n'}(i-i',j+j',0)\\
G_{IM_{xy}}^{n-n'}(i-i',j,j') &= G_{xy}^{n-n'}(i-i',j-j',0) + G_{xy}^{n-n'}(i-i',j+j',0)\\
G_{IM_{yx}}^{n-n'}(i-i',j,j') &= G_{yx}^{n-n'}(i-i',j-j',0) - G_{yx}^{n-n'}(i-i',j+j',0)
\end{aligned}
\tag{6}
$$

Then, the current on the antenna can be computed as:

$$
\begin{bmatrix} J_{xa} \\ J_{ya} \end{bmatrix}_{i,j}^{n} = -\varepsilon \begin{bmatrix} E_{\mathrm{inc}\,x} \\ E_{\mathrm{inc}\,y} \end{bmatrix}_{i,j}^{n} - \varepsilon \sum_{n'=0}^{n-1} \sum_{i',j'} \begin{bmatrix} G_{IMxx} & G_{IMxy} \\ G_{IMyx} & G_{IMyy} \end{bmatrix}_{i-i',j,j'}^{n-n'} \begin{bmatrix} J_{xa} \\ J_{ya} \end{bmatrix}_{i',j'}^{n'} \tag{7}
$$

4. RESULTS AND DISCUSSION

The spatial and time increments have been selected as $\Delta x = \Delta y = \Delta z = 0.25\,\mathrm{mm}$ and $c\ \Delta\ t = 0.5\ \Delta\ x$, respectively. Computations are performed only on the surface of the antenna with the spatial grid of 95×80. The antenna is excited by the incident Gaussian electric field in *y*-direction at feed point. In order to accelerate the calculation of multidimensional convolutions of (6), we have utilized fast Fourier transform for calculation of spatial convolutions of Eq. (7) [9]. The density of current on the antenna at time step n is computed from the time iteration of the (7) in terms of current at previous time steps. The simulated and measured return loss of the proposed antenna without slots, whose parameters are kept the same as those in Table 1, is compared in Figure 3. The antenna has a very wide bandwidth of over 145% in the frequency range from 2.6 to 17.8 GHz. Figure 4 shows the

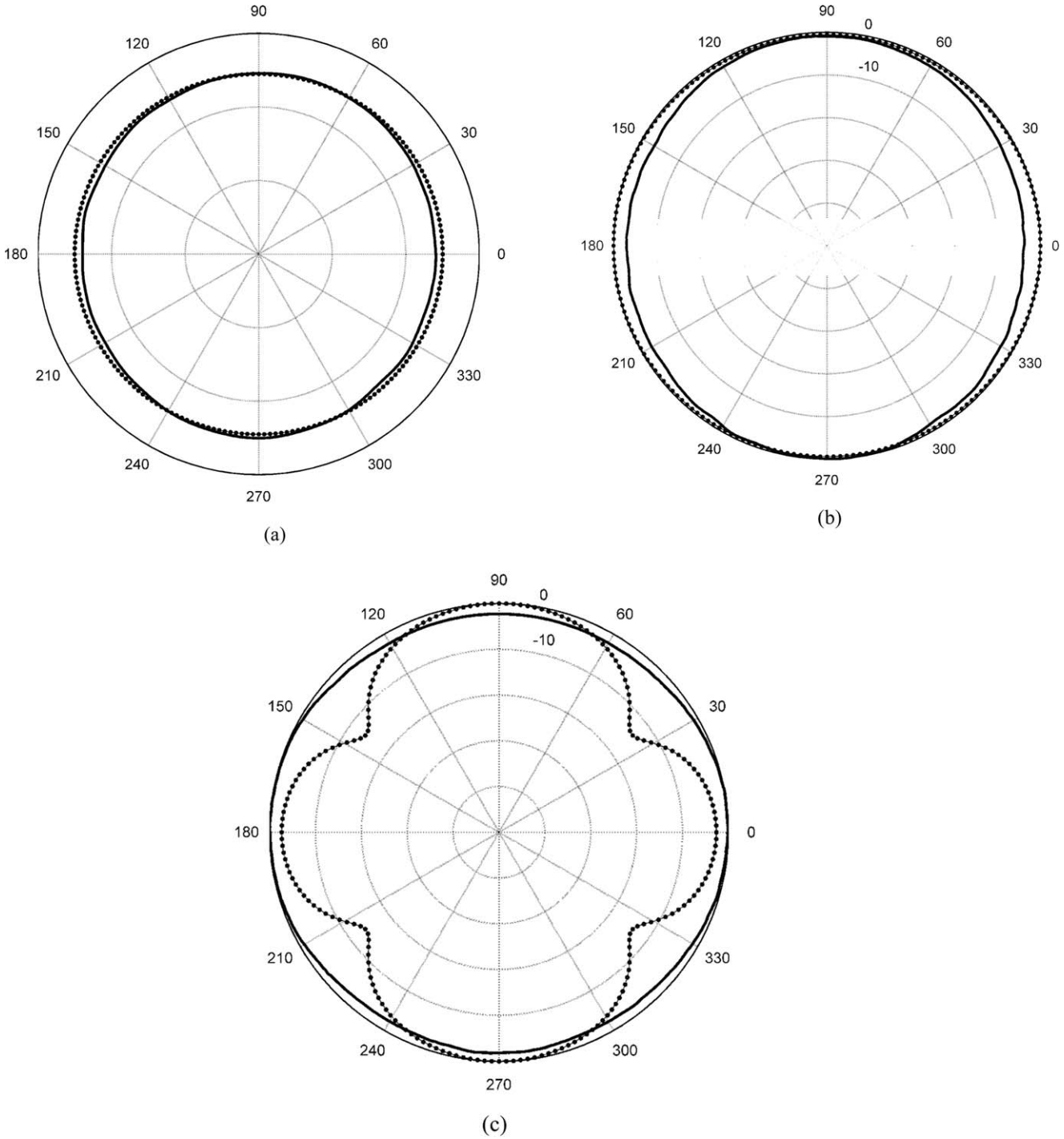

Figure 7 Simulated and measured pattern of the antenna in *x-z* plane at (a) 3 GHz, (b) 6.5 GHz, and (c) 9 GHz. (solid line: measurement, dotted line: simulation)

simulated and measured return loss of the antenna having proposed slots. The measured result agrees reasonably with the simulated result. The discrepancy is expected from two reasons. First, in simulation, the thickness of the antenna has been ignored. Second, a finer mesh can be modeled slots more accurately, especially, in the first notched band. The measured notches frequency band characteristics are occurred from 3.38 to 3.7 GHz and from 5.18 to 5.84 GHz. The far-field radiation pattern can be also obtained by applying fast Fourier transform to the time-domain current distribution. The measured and simulated results of radiation pattern at frequency 3, 6.5, and 9 GHz are compared from Figures 5 to 7. The finite ground plane effects on the measured radiation patterns are seen.

5. CONCLUSION

In conclusion, we have designed dual band-notched slots for the UWB metal plate monopole antenna with trident feeding. DGF method has been selected as a simulation tool for the analysis of the antenna. This technique computes time-domain current distribution on the antenna regardless of the computation free space around the antenna, which occurs in the FDTD method.

Furthermore, unlike the method of moments, the wide band frequency response of the antenna can be obtained through single run of the code.

REFERENCES

1. M.J. Ammann, Control of the impedance bandwidth of wideband planar antenna using a beveling technique, Microwave Opt Technol Lett 30 (2001), 229–232.
2. S.M. Mazinani and H.R. Hassani, A novel broadband plate-loaded planar monopole antenna, IEEE Antennas Wireless Propag Lett 8 (2009), 1123–1126.
3. M.J. Ammann and Z.N. Chen, A wide-band shorted planar monopole with bevel, IEEE Trans Antennas Propag 51 (2003), 901–903.
4. S.W. Su, K.L. Wong, and C.L. Tang, Ultra wideband square planar monopole antenna for IEEE 802.16a operation in the 2–11 GHz band, Microwave Opt Technol Lett 42 (2004), 463–466.
5. K.L. Wong, C.H. Wu, and S.W. Su, Ultrawide-band square planar metal-plate monopole antenna with a trident-shaped feeding strip, IEEE Trans Antennas Propag 53 (2005), 1262–1269.
6. J. Vazquez and C.G. Parini, Discrete Green's function formulation of FDTD method for electromagnetic modeling, Electron Lett 35 (1999), 554–555.
7. J. Vazquez and C.G. Parini, Antenna modeling using discrete Green's function formulation of FDTD method, Electron Lett 35 (1999), 1033–1034.
8. W. Ma, M.R. Rayner, and C.G. Parini, Discrete Green's function formulation of the FDTD method and its application in antenna modeling, IEEE Trans Antennas Propag 53 (2005), 339–364.
9. S. Mirhadi, M. Soleimani, and A. Abdolali, An FFT-based approach in acceleration of discrete Green's function method for antenna analysis, Prog Electromagn Res M 29 (2013), 17–28.

DESIGN OF A CIRCULAR RING MONOPOLE ANTENNA WITH INVERTED T-STRIP LINE FOR DUAL-BAND OPERATION

Yongseok Seo,[1] Hyeonjin Lee,[2] and Yeongseog Lim[1]

[1] Department of Electronics and Computer Engineering, Chonnam National University, 300, Yongbong-Dong, Buk-gu, Gwangju, 500-757, South Korea; Corresponding author: on1yys82@gmail.com

[2] Department of Electrical and Electronics, Dongkang College University, Gwangju, South Korea

Received 9 January 2013

ABSTRACT: *A novel and simple design of a coplanar waveguide-fed multiband antenna formed by a circular ring monopole antenna is investigated for DCS/PCS/UMTS/LTE_CN/WLAN. The impedance bandwidths that were achieved reach to about 0.84 GHz (1.68–2.52 GHz) 42.0% at the center frequency of 2.0 and 0.72 GHz (5.14–5.86 GHz) 13.1% at the center frequency of 5.5 GHz. Moreover, the resonant characteristics of the antenna can be tuned by using the inverted T-strip line. Experimental results exhibit that the proposed circular ring antenna creates a monopole-like pattern in the E-plane and an omnidirectional radiation pattern in the H-plane, so it is well suitable to meet DCS/PCS/UMTS/LTE_ CN/WLAN operations.* © 2013 Wiley Periodicals, Inc. Microwave Opt Technol Lett 55:2174–2176, 2013; View this article online at wileyonlinelibrary.com. DOI 10.1002/mop.27761

Key words: *monopole antenna; WLAN; dual-band; antenna*

1. INTRODUCTION

Wireless communication devices play a very important part in our daily lives. Portable devices have become very popular to consumers and they attract great interest from major manufacturers [1–3]. Multiband antennas are able to provide multiple reception and transmission functionalities. Therefore, it is very desirable to have a single antenna which uses a single feed point that covers multiple frequency bands. The designed antennas are expected to be compact, simple, and integrated well with other communication devices. Conventional antennas such as trident-shaped monopole antenna [4], modified fork-shaped monopole antenna [5], and planar monopole antenna [6] are presented. However, these antennas have complicated structures and are printed on both sides of the substrate, which increases manufacturing difficulty and cost. In this article, we propose a coplanar waveguide (CPW)-fed circular ring monopole antenna suitable for use in DCS (1710–1880 MHz), PCS (1850–1990 MHz), UMTS (1920–2170 MHz), LTE_CN (2305–2400 MHz), and WLAN (2400–2484 MHz)/(5150∼5825 MHz). The proposed antenna is particularly easy to manufacture and this is due to its single dielectric and single metal-layer geometry. Details of the antenna design are described and the prototypes of the proposed antenna for multifrequency operation have been constructed and tested. Moreover, the comparisons between the simulated and measured results of the obtained antenna are presented and discussed.

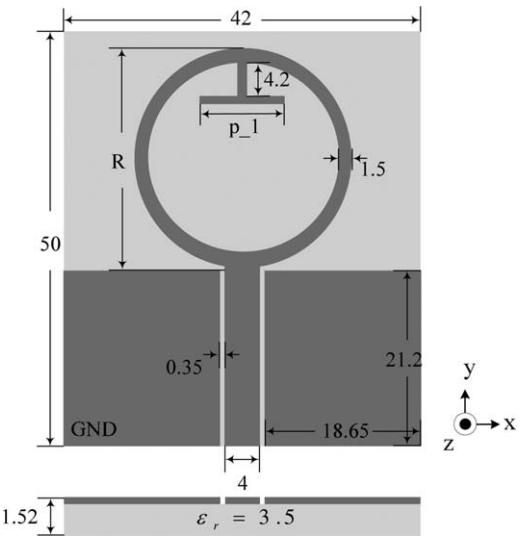

Figure 1 Geometry of the proposed antenna

2. ANTENNA DESIGN AND EXPERIMENTAL RESULTS

The geometry of the proposed antenna is shown in Figure 1. The antenna consists of a circular ring, a CPW and symmetrically finite ground planes. The proposed antenna is fabricated on a low-cost Teflon substrate of relative permittivity 3.5 and a loss tangent of 0.0018. In order to provide DCS/PCS/UMTS/LTE_CN/WLAN operations, a circular ring is chosen as a radiating element and it is easily fed by a CPW microstrip feedline. The overall dimensions of the proposed antenna are $42 \times 50 \times 1.52\,\text{mm}^3$ and it includes the feed structure. The radiation element of the proposed antenna is a circular ring with width of 1.5 mm and it provides a current path for $R = 26.5$ mm ring resonance at 2.0 GHz. The fundamental resonant path of the circular ring monopole can be calculated as:

$$R = \frac{c}{4f_1\sqrt{\varepsilon_{\text{eff}}}}$$

Where c is the speed of light, ε_{eff} is the equivalent dielectric constant, and $f_1 = 2$ GHz denotes the fundamental resonant